Scientific Research Publishing

Journal of High Energy Physics, Gravitation and Cosmology, 2026, 12(2), 762-781
https://www.scirp.org/journal/jhepgc
ISSN Online: 2380-4335
ISSN Print: 2380-4327

Constraints on Dark Photon and Dark Z Model Parameters in the B and K Meson Decays

Ahmed Rashed

Department of Physics, Shippensburg University of Pennsylvania, Shippensburg, PA, USA
Email: AMRashed@ship.edu

How to cite this paper: Rashed, A. (2026) Constraints on Dark Photon and Dark Z Model Parameters in the B and K Meson Decays. *Journal of High Energy Physics, Gravitation and Cosmology*, **12**, 762-781.
https://doi.org/10.4236/jhepgc.2026.122040

Received: December 9, 2025
Accepted: March 24, 2026
Published: March 27, 2026

Copyright © 2026 by author(s) and Scientific Research Publishing Inc.
This work is licensed under the Creative Commons Attribution International License (CC BY 4.0).
http://creativecommons.org/licenses/by/4.0/

Open Access

Abstract

The study investigates flavor-changing neutral current (FCNC) decays of B and K mesons in the context of a dark $U(1)_D$ model with a dark photon/dark Z mass between 10 MeV and 2 GeV. While the model improves the fit to certain decay distributions, such as $B \to K^{(*)}\ell^+\ell^-$ and $B_s \to \phi\mu^+\mu^-$, it is ruled out by stringent experimental constraints, including atomic parity violation, $K^+ \to \mu^+ + \text{invisible}$, and $B_s - \bar{B}_s$ mixing. To address these constraints, the model is extended with three modifications: allowing additional invisible decays of Z_D, introducing a direct vector coupling of Z_D to muons, and including a direct coupling of Z_D to both muons and electrons, with fine-tuning to cancel the mixing-induced coupling to electrons. Among these extensions, only the third scenario, involving fine-tuned electron coupling, remains consistent with all experimental constraints.

Keywords

Dark Matter, B-Physics, FCNC

1. Introduction

Flavor-changing neutral currents (FCNCs) serve as sensitive probes for new physics (NP) and strongly constrain extensions of the Standard Model (SM). This study examines how recent FCNC measurements in the B-meson system constrain models involving a light gauge boson, focusing on the dark $U(1)_D$ model, which predicts either a dark photon or a dark Z (often referred to as Z') depending on its couplings. A dark photon arises solely through kinetic mixing

with the electromagnetic field strength [1], while a dark Z also involves mass mixing with SM gauge bosons [2] [3]. Both scenarios involve loop-induced FCNC processes, with significant contributions from up-type quarks in B decays due to the large top quark mass, while D decays are suppressed by down-type quark contributions.

A key feature of models with light mediators is the q^2 -dependent Wilson coefficients (WCs) they generate, distinguishing them from heavy NP that can be integrated out. The role of light mediators in $b \to s\ell^+\ell^-$ transitions has been extensively explored [4]-[15]. This study focuses on a vector mediator Z_D with mass $0.01 < M_{Z_D}\,\text{GeV} < 2$, considering both on-shell and off-shell decays. FCNC processes for both dark photon and dark Z scenarios are analyzed, incorporating leptonic, hadronic, and invisible decays of Z_D. This work also accounts for hadronic decay contributions, often overlooked, and corrects earlier results [16] by including the q^2 -independent dark Z monopole operator.

The model is extended to include direct couplings of Z_D to muons, and to both muons and electrons, in addition to mixing-induced couplings. Invisible Z_D decays to dark sector particles are also considered. Constraints from $b \to s\ell^+\ell^-$ data and other low-energy experiments are used to limit the model's parameter space.

2. Formalism

The Z_D boson is associated with a broken $U(1)_D$ gauge symmetry in the dark sector, coupling to the Standard Model (SM) through kinetic mixing with $U(1)_Y$. The gauge Lagrangian is written as [1] [3]

$$\mathcal{L}_{\text{gauge}} = -\frac{1}{4}B_{\mu\nu}B^{\mu\nu} + \frac{1}{2}\frac{\varepsilon}{\cos\theta_W}B_{\mu\nu}Z_D^{\mu\nu} - \frac{1}{4}Z_{D\mu\nu}Z_D^{\mu\nu},$$

with ε as the kinetic mixing parameter. After diagonalizing the gauge sector, Z_D couples to the SM via

$$\mathcal{L}_D^{\text{em}} \supset e\varepsilon Z_D^{\mu}J_{\mu}^{\text{em}} - ie\varepsilon\left[\!\left[Z_D W^+W^-\right]\!\right],$$

with

$$\begin{aligned}\left[\!\left[Z_D W^+W^-\right]\!\right] &= \varepsilon_{Z_D}^{\mu}(k_1)\varepsilon_{W^+}^{\nu}(k_2)\varepsilon_{W^-}^{\lambda}(k_3)\\ &\times\left[(k_1-k_2)_{\lambda}\,g_{\mu\nu} + (k_2-k_3)_{\mu}\,g_{\nu\lambda} + (k_3-k_1)_{\nu}\,g_{\lambda\mu}\right].\end{aligned} \tag{1}$$

where the interaction includes both the electromagnetic current and terms involving W -bosons. If $U(1)_D$ is broken by a scalar charged under the SM, mass mixing occurs, leading to physical eigenstates expressed as [2] [3]

$$Z = Z^0\cos\xi - Z_D^0\sin\xi,\quad Z_D = Z^0\sin\xi + Z_D^0\cos\xi,$$

where ξ parameterizes the mixing. The mass mixing induces couplings between Z_D and SM fields, as described by

$$\mathcal{L}_D^Z \supset \frac{g}{\cos\theta_W}\varepsilon_Z Z_D^{\mu}J_{\mu}^Z - ig\cos\theta_W\varepsilon_Z\left[\!\left[Z_D W^+W^-\right]\!\right],$$

with $\varepsilon_Z \equiv \frac{1}{2}\tan 2\xi$. The model parameters are ε, ε_Z, and M_{Z_D} (mass of the Z_D boson), constrained by experimental data [17]-[19].

Flavor-changing neutral current (FCNC) decays such as $b \to sZ_D$ occur via loop diagrams involving $d_i \to d_j Z_D$. The effective Hamiltonian includes monopole and dipole operators with Wilson coefficients

$$H_{\text{eff}} \supset \left(\bar{F}_a' \gamma^\mu P_{L,R} F_b\right)\left[\left(E_{a,b}^{0,c}\right)_{L,R} g^{\mu\nu} + \left(g^{\mu\nu}q^2 - q^\mu q^\nu\right)\left(E_{a,b}^{2,c}\right)_{L,R}\right]V_\nu^c,$$

and

$$H_{\text{eff}} \supset \left(\bar{F}_a' \sigma^{\mu\nu} P_{L,R} F_b q_\mu V_\nu^c\right)\left(M_{a,b}^{1,c}\right)_{L,R}.$$

The hadronic part of the amplitude is expressed as

$$\begin{aligned}\mathcal{M}_{Z_D} = &\left\langle \mathcal{H}_2 \middle| \bar{d}_i \gamma_\mu P_{L/R} d_j \middle| \bar{\mathcal{H}}_1 \right\rangle \left[\left\{\left(E_{c_1,c_2}^{0,A}\right)_{L/R} + \left(E_{c_1,c_2}^{0,Z}\right)_{L/R}\right\} g^{\mu\nu}\right. \\ &\left. + \left\{\left(E_{c_1,c_2}^{2,A}\right)_{L/R} + \left(E_{c_1,c_2}^{2,Z}\right)_{L/R}\right\}\left(g^{\mu\nu}q^2 - q^\mu q^\nu\right)\right] V_\nu^{Z_D} \\ &+ \left\langle \mathcal{H}_2 \middle| \bar{d}_i i q_\mu \sigma^{\mu\nu} P_{L/R} d_j \middle| \bar{\mathcal{H}}_1 \right\rangle \left\{\left(M_{c_1,c_2}^{1,A}\right)_{L/R} + \left(M_{c_1,c_2}^{1,Z}\right)_{L/R}\right\} V_\nu^{Z_D},\end{aligned} \tag{2}$$

with $V_\nu^{Z_D}$ is the polarization vector of Z_D and the hadronic currents.

Amplitudes for FCNC processes ($b \to sZ_D, s \to dZ_D, b \to dZ_D$) are computed using the Peng4BSM@LO package [20].

Semileptonic $b \to s\ell^+\ell^-$ decays involve effective Hamiltonians of the form

$$\mathcal{H}_{\text{eff}}^{bs\ell\ell} = -\frac{4G_F}{\sqrt{2}}\frac{e^2}{16\pi^2} V_{tb}V_{ts}^* \sum_i \left(\mathcal{C}_i \mathcal{O}_i + \mathcal{C}_i' \mathcal{O}_i'\right),$$

where $\mathcal{C}_i'$ are the WCs corresponding to the dimension six operators $\mathcal{O}_i'$ with Wilson coefficients $\mathcal{C}_{9,\ell}$ and $\mathcal{C}_{10,\ell}$ given by

$$\begin{aligned}\mathcal{C}_{9,\ell} = &\left(\left(E_{c_1,c_2}^{0,Z}\right)_L + \left\{\left(E_{c_1,c_2}^{2,A}\right)_L + \left(E_{c_1,c_2}^{2,Z}\right)_L\right\} q^2\right) \\ &\times \left(\frac{1}{q^2 - M_{Z_D}^2 + i\Gamma_{Z_D} M_{Z_D}}\right)\left(e\varepsilon + \frac{g}{c_W}\varepsilon_Z g_V^\ell\right),\end{aligned} \tag{3}$$

$$\begin{aligned}\mathcal{C}_{10,\ell} = &\left(\left(E_{c_1,c_2}^{0,Z}\right)_L + \left\{\left(E_{c_1,c_2}^{2,A}\right)_L + \left(E_{c_1,c_2}^{2,Z}\right)_L\right\} q^2\right) \\ &\times \left(\frac{1}{q^2 - M_{Z_D}^2 + i\Gamma_{Z_D} M_{Z_D}}\right)\left(\frac{g}{c_W}\varepsilon_Z g_A^\ell\right),\end{aligned} \tag{4}$$

$$\mathcal{C}_{9,\ell}' = \mathcal{C}_{10,\ell}' = 0, \tag{5}$$

where $g_V^\ell = \left(-1 + 4s_W^2\right)/2$ and $g_A^\ell = -1/2$ are the vector and axial vector coupling constants for the SM $Z\ell\ell$ interaction; s_W and c_W are the sine and cosine of θ_W, respectively. When obvious, we suppress the ℓ subscript in the WCs.

If M_{Z_D} lies within the kinematic range of the decay, on-shell Z_D contributions can significantly affect branching fractions [9].

For Z_D, decays to e^+e^-, $\mu^+\mu^-$, and hadronic final states are considered. Partial widths for leptonic and hadronic decays are computed using vector meson

dominance (VMD) models [21]-[23], with the hadronic width estimated as

$$\Gamma\left(Z_D \to \mathcal{H}\right) = \Gamma\left(Z_D \to \mu^+\mu^-\right) \times \mathcal{R}_\mu^{\mathcal{H}},$$

where $\mathcal{R}_\mu^{\mathcal{H}}$ is derived from experimental data [24].

3. Models

We study three different cases of the light Z_D model as specified below.

- **Case A**: This is the dark photon and dark Z model. The model has two mixing parameters (ε and ε_Z) and the mass M_{Z_D} .
- **Case B**: A muonphilic Z_D in which Case A is extended with an additional direct interaction of the dark Z with muons

$$\mathcal{L}_D^Z \supset g_D^\mu \bar{\mu}\gamma_\alpha \mu Z_D^\alpha. \tag{6}$$

This scenario has an additional free parameter g_D^μ .

The direct interaction with muons could potentially emerge from a gauged $U(1)_{L_\mu - L_\tau}$ symmetry or similar frameworks. For instance, in Ref. [25] discusses how such a symmetry introduces a new gauge boson that couples to muons and taus, providing a UV completion pathway.

- **Case C**: Case A is extended with additional direct interactions of the dark Z with both electrons and muons

$$\mathcal{L}_D^Z \supset g_D^e \bar{e}\gamma_\alpha e Z_D^\alpha + g_D^\mu \bar{\mu}\gamma_\alpha \mu Z_D^\alpha. \tag{7}$$

We assume g_D^e is fine-tuned so that it cancels the coupling of Z_D to electrons via mixing. Then, all observables for the electron mode are described by the SM only.

The coupling to both muons and electrons is fine-tuned, the scenario might originate from a more intricate symmetry-breaking pattern in the dark sector. Ref. [26] explores mechanisms where a hidden $SU(2)$ gauge symmetry is broken by a scalar multiplet, leading to mass relations among gauge bosons and potential fine-tuning in couplings.

4. Constraints

4.1. B_s Mixing

B meson mixing is a significant tool for probing new physics, providing stringent constraints on theoretical models. In the Standard Model (SM), the mixing originates from a box diagram involving a W boson and a top quark [27]. The dominant SM contribution to the mass difference between B_s^0 and $\overline{B}_s^0$ mesons depends on QCD corrections, the top quark mass [28], and hadronic parameters like the decay constant and bag parameter [29]. Lattice QCD calculations have refined these parameters [30].

New Physics (NP) contributions, such as from a potential dark Z_D boson, modify the mass difference. These contributions depend on the Z_D mass and coupling constants [8]. The experimental mass difference aligns closely with SM

predictions [24] [31], placing tight constraints on NP parameters. Notably, lighter Z_D bosons require smaller couplings to remain consistent with observations, disallowing certain parameter combinations, particularly for Z_D masses below 60 MeV and couplings above 0.001. These findings underscore the sensitivity of $B_s^0 - \overline{B}_s^0$ mixing to new physics.

We plot the sensitivity of $B_s^0 - \overline{B}_s^0$ mixing to ϵ_Z, Δ_{mix}, as a function of the dark Z mass for different values of ε_Z in **Figure 1**. It is evident that lighter Z_D require smaller values of ε_Z for Δ_{mix} to lie within the 2σ uncertainty of the SM prediction. We find that $\varepsilon_Z \geq 0.001$ is disallowed for $M_{Z_D} \leq 60$ MeV.

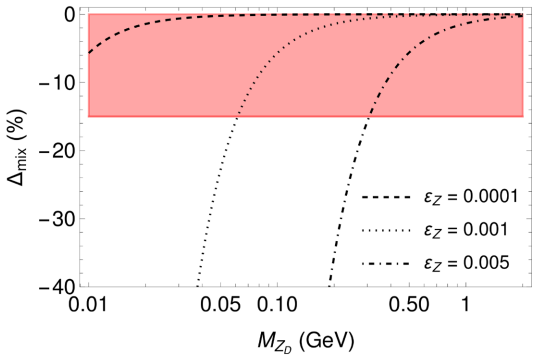

Figure 1. Sensitivity of $B_s^0 - \overline{B}_s^0$ mixing to ε_Z as a function of M_{Z_D}. At leading order Δ_{mix} is independent of ε. The red band is the uncertainty in Δ_{mix} taken to be the 2σ lower uncertainty in $\Delta M_{B_s}^{SM}$.

4.2. $B_s \to \mu^+\mu^-$

The rare decay $B_s \to \mu^+\mu^-$ is a crucial probe for new physics. Its branching fraction depends on Standard Model (SM) parameters and possible contributions from new physics. In the Z_D model, contributions from scalar and pseudoscalar Wilson coefficients are absent, leaving the dominant effect from $\mathcal{C}_{10}$ [32].

The SM prediction for the branching fraction is $\mathcal{B}\left(B_s^0 \to \mu^+\mu^-\right)^{SM} = (3.67 \pm 0.15) \times 10^{-9}$ [33] [34], while the experimental measurement from LHCb is $\mathcal{B}\left(B_s^0 \to \mu^+\mu^-\right)^{LHCb} = \left(3.09^{+0.46+0.15}_{-0.43-0.11}\right) \times 10^{-9}$ [35]. The close agreement between these values constrains potential new physics contributions, highlighting the importance of precision in both theoretical predictions and experimental measurements.

The Z_D contribution to this rare decay is shown in **Figure 2**. Since the decay rate depends only on the new axial-vector interaction of the dark Z, it is independent of ε. It is evident that ε_Z as large as 0.01 is allowed by the data at the 3σ confidence level (CL).

4.3. $B \to K^{(*)}\nu\bar{\nu}$

The decays $B \to K^{(*)}\nu\bar{\nu}$ are sensitive probes for new physics, particularly in the

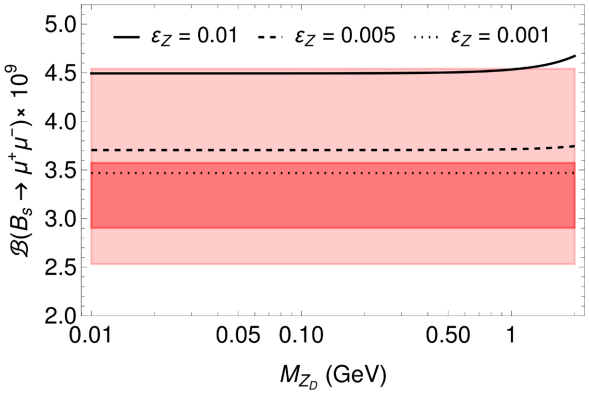

Figure 2. Branching fraction for $B_s \to \mu^+\mu^-$ for different values of ε_Z. The horizontal red (light red) band denotes the 1σ (3σ) allowed region from experiment [35]. The decay rate does not depend on ε.

context of the Z_D model. These decays involve the on-shell production of Z_D in B decay, followed by $Z_D \to \nu\bar{\nu}$ [36]. The effective interaction strengths and form factors governing these decays are derived from loop functions, and their detailed expressions are available in [37].

The Standard Model (SM) predicts branching fractions of $\mathcal{B}\left(B^+ \to K^+\nu\bar{\nu}\right)_{SM} = (4.4 \pm 0.7) \times 10^{-6}$ and $\mathcal{B}\left(B^0 \to K^{*0}\nu\bar{\nu}\right)_{SM} = (11.6 \pm 1.1) \times 10^{-6}$ [38]. A recent search by Belle II for $B^+ \to K^+\nu\bar{\nu}$ sets a 90% confidence level (CL) upper bound of $\mathcal{B}\left(B^+ \to K^+\nu\bar{\nu}\right) < 4.1 \times 10^{-5}$ [39], and the weighted average from existing data is $\mathcal{B}\left(B^+ \to K^+\nu\bar{\nu}\right)_{WA} = (1.1 \pm 0.4) \times 10^{-5}$ [38], showing a slight enhancement over the SM prediction. However, this enhancement should not yet be interpreted as evidence for new physics.

For $B \to K^*\nu\nu$, the most recent 90% CL upper bound from Belle is $\mathcal{B}\left(B^0 \to K^{*0}\nu\bar{\nu}\right) < 1.8 \times 10^{-5}$ [40]. These results impose constraints on new physics scenarios while leaving room for further exploration.

In **Figure 3**, we plot the branching fractions for some benchmark values of ε_Z. We find that they are more than an order of magnitude smaller than the respective upper bounds even for ε_Z as large as 0.1.

4.4. Kaon Decay and Mixing

The flavor-changing decays $K \to \pi\nu\bar{\nu}$ are governed by the $s \to d\nu\bar{\nu}$ transition. The key decay modes are $K^+ \to \pi^+\nu\bar{\nu}$ and $K_L \to \pi^0\nu\bar{\nu}$. The most recent measurement from the NA62 experiment gives $\mathcal{B}\left(K^+ \to \pi^+\nu\bar{\nu}\right) = \left(10.6^{+4.0}_{-3.4} \pm 0.9\right) \times 10^{-11}$ [41], while the KOTO experiment places a 90% confidence level (CL) upper bound of $\mathcal{B}\left(K_L \to \pi^0\nu\bar{\nu}\right) < 4.9 \times 10^{-9}$ [42]. These results align with the Standard Model (SM) predictions of $\mathcal{B}\left(K^+ \to \pi^+\nu\bar{\nu}\right)_{SM} = (8.4 \pm 1.0) \times 10^{-11}$ and

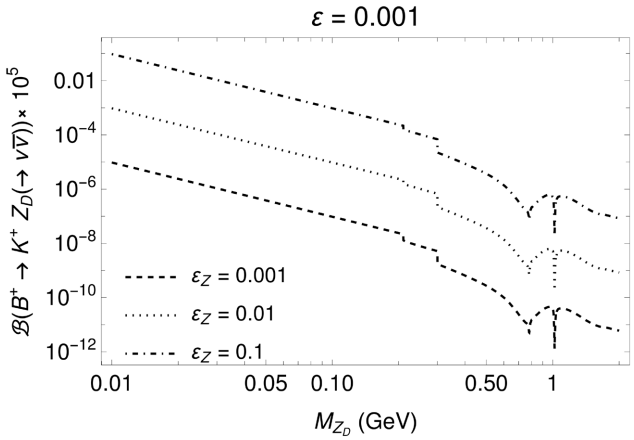

Figure 3. Branching fraction of $B \to K^{(*)}\nu\bar{\nu}$ as a function of the Z_D mass for three values of ε_Z and $\varepsilon = 0.001$.

$\mathcal{B}\left(K_L \to \pi^0\nu\bar{\nu}\right)_{SM} = (3.4 \pm 0.6)\times 10^{-11}$ [43] [44]. The two modes are related through the Grossman-Nir bound, which limits $\mathcal{B}\left(K_L \to \pi^0\nu\bar{\nu}\right)$ based on $\mathcal{B}\left(K^+ \to \pi^+\nu\bar{\nu}\right)$ [45].

In the context of new physics, including the Z_D model, contributions to these decays are resonant but highly suppressed due to the weak $s \to dZ_D$ transition. Consequently, the branching fractions remain small even for relatively large Z_D coupling parameters ($\epsilon_Z \sim 0.01$).

Neutral kaon oscillations ($K^0 \leftrightarrow \bar{K}^0$) are also relevant, with a mass difference ΔM_K that matches the SM prediction of $3.484(6)\times 10^{-12}$ MeV [32]. The dominant SM contribution arises from loop-level processes with QCD corrections and hadronic parameters, while new physics contributions from the Z_D model, for example, are found to be negligible under typical parameter values, such as $M_{Z_D} = 10$ MeV and $\epsilon_Z = 0.001$. Thus, ΔM_K does not strongly constrain this model.

4.5. Radiative $K^+ \to \mu^+\nu_\mu Z_D$ Decays

The three-body decay $K^+ \to \mu^+\nu_\mu Z_D$ serves as a radiative correction to the standard $K^+ \to \mu^+\nu_\mu$ decay, where the dark boson Z_D is emitted from the muon leg and subsequently decays invisibly. This decay is relevant for scenarios where the dark boson mass is below $2m_\mu$, allowing it to be produced on-shell. Experimental constraints on this process have been established by the NA62 experiment, which sets a 90% confidence level upper limit on the branching fraction for $K^+ \to \mu^+\nu\nu\bar{\nu}$ at 1.0×10^{-6} [46]. This bound imposes restrictions on the coupling parameters of the dark boson in various model scenarios.

In one scenario, referred to as Case A, where the emission is suppressed by mixing parameters, the branching fraction remains below the experimental limit even for relatively large couplings, as illustrated in the left panel of **Figure 4**. Conversely, in Case B, where the direct coupling g_D^μ dominates, the branching

fraction increases with g_D^μ, necessitating $g_D^\mu < 0.01$ to remain consistent with the data. This behavior is shown in the right panel of Figure 4. The interplay between mixing and direct coupling highlights distinct constraints depending on the underlying assumptions of the model.

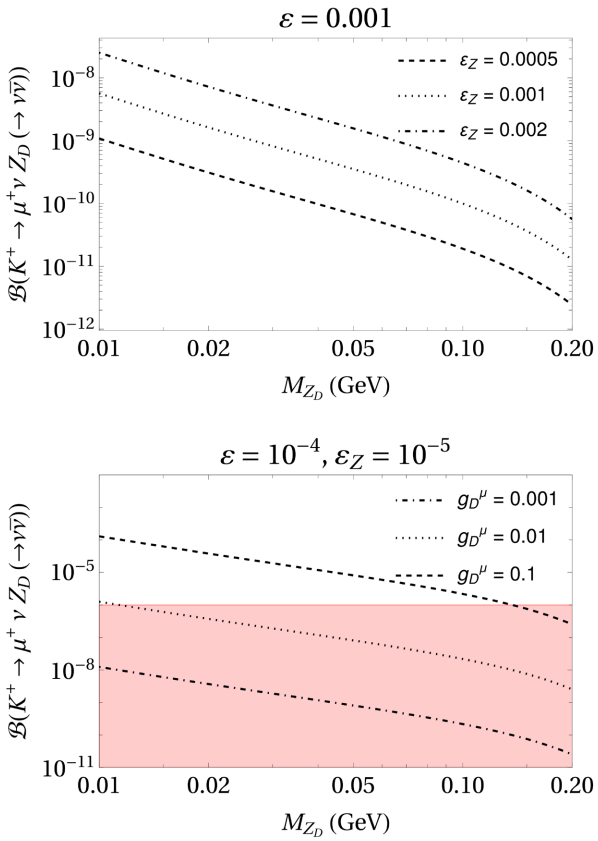

Figure 4. Dependence of the $K^+ \to \mu^+ +$ invisible branching fraction on the mixing parameters in Case A (left) and on the direct coupling g_D^μ in Case B (right). The red shaded region shows the 90% CL upper limit on the branching fraction.

In addition to invisible decays, the dark boson Z_D can also decay into visible final states, such as e^+e^-. This contributes to the decay $K^+ \to \mu^+ \nu e^+ e^-$, for which the experimentally measured branching fraction is $(7.06 \pm 0.31) \times 10^{-8}$ [24] [47] for invariant electron-positron masses above 145 MeV. Within the context of Case B, the coupling g_D^μ can enhance the branching fraction significantly for $145 < M_{Z_D} < 200$ MeV when $\epsilon_Z < \epsilon$ and Z_D predominantly decays to e^+e^-. This dependence is illustrated in Figure 5, where the constraints from data are clearly visible. Notably, these constraints do not apply to scenarios like Case C, where Z_D lacks coupling to electrons.

Overall, the analysis of both invisible and visible decay modes of the dark boson provides stringent experimental constraints on its properties, demonstrating how rare kaon decays can serve as sensitive probes of new physics.

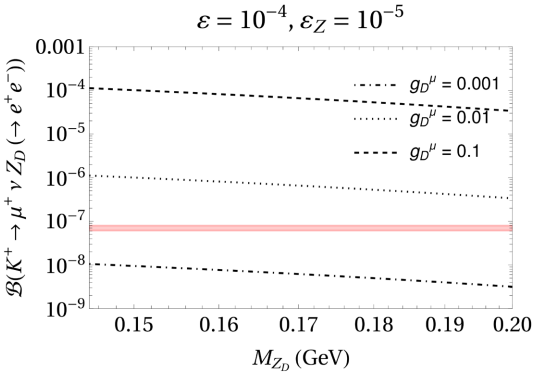

Figure 5. Dependence of the $K^+ \to \mu^+ \nu e^+ e^-$ branching fraction on g_D^μ in Case B. The red shaded region shows the 3σ interval of the branching fraction.

4.6. Radiative $\pi^+ \to \mu^+ \nu_\mu Z_D$ Decays

The decay process $\pi^+ \to \mu^+ \nu_\mu Z_D$, analogous to radiative kaon decay, can be enhanced when the dark boson Z_D mass satisfies $0 < M_{Z_D} < m_\pi - m_\mu$. The PIENU experiment provides constraints on this process by setting an upper bound on the ratio $R^{\pi\mu\nu X} = \Gamma\left(\pi^+ \to \mu^+ \nu_\mu X\right) / \Gamma\left(\pi^+ \to \mu^+ \nu_\mu\right)$, where X is an invisible decay product [48], in the mass range $0 < M_X < 33.9$ MeV perimental bound is used to constrain the parameters of the dark boson.

The decay rate depends on the coupling structure. In Case A, it is suppressed by mixing parameters, while in Cases B and C, it scales with $\left(g_D^\mu\right)^2$. The amplitude squared for the process is derived from the general interaction and is adjusted for pion decay by substituting the relevant constants (e.g., $f_K \to f_\pi$, $V_{us} \to V_{ud}$, and $m_K \to m_\pi$).

Figure 6 illustrates the relationship between $R^{\pi\mu\nu X}$ and g_D^μ, with experimental limits from PIENU shown for two ranges of muon kinetic energy: $T_\mu > 1.2$ MeV (solid black curve) and $T_\mu < 1.2$ MeV (solid red curve). The results indicate that $g_D^\mu < 0.1$ is consistent with the data for $M_{Z_D} < 34$ MeV if the dark Z does not predominantly decay to neutrinos (*i.e.*, $\epsilon_Z \ll \epsilon$). However, for $\epsilon_Z \geq \epsilon$, where $B\left(Z_D \to \nu\bar{\nu}\right)$ is significant, $g_D^\mu \geq 0.1$ is excluded for $M_{Z_D} < 15$ MeV. This highlights the sensitivity of $\pi^+ \to \mu^+ \nu_\mu Z_D$ decays to the coupling parameters and branching ratios of the dark boson.

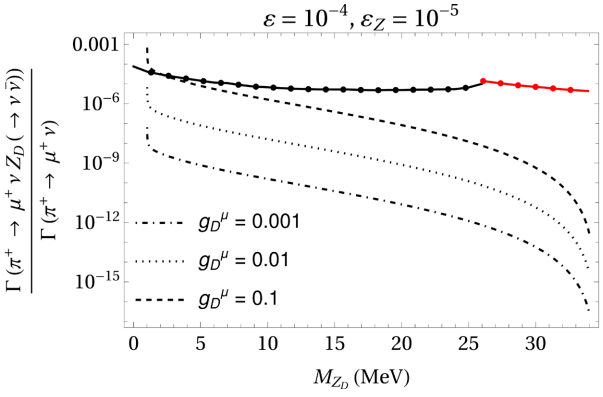

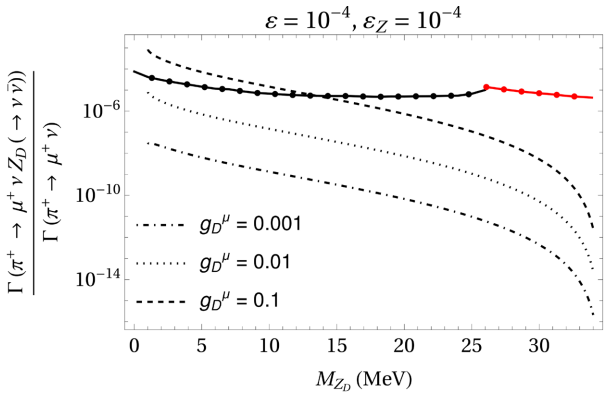

Figure 6. Dependence of $R^{\pi\mu\nu X} = \Gamma\left(\pi^+ \to \mu^+ \nu_\mu Z_D(\to \nu\bar{\nu})\right) / \Gamma\left(\pi^+ \to \mu^+ \nu_\mu\right)$ on g_D^μ for $\varepsilon_Z = 10^{-5}$ (left) and 10^{-4} (right). The black and red solid curves punctuated with points show the 90% CL upper limit from PIENU for the muon kinetic energy ranges, $T_\mu > 1.2$ MeV and $T_\mu < 1.2$ MeV, respectively.

4.7. Atomic Parity Violation

The dark boson Z_D can couple to first-generation Standard Model (SM) fermions via mixing, leading to stringent constraints from atomic parity-violating (APV) observables. These interactions affect the weak charge Q_W of the proton and certain nuclei, such as cesium (133Cs), whose measured values are $Q_W^{p,exp} = 0.0719(45)$ and $Q_W^{^{133}\mathrm{Cs},exp} = -72.82(42)$ [44] [49] [50], respectivelyn-fluenced by modifications to the Fermi constant G_F and the weak mixing angle θ_W, both of which are altered by the dark boson interaction. The parameters ρ_d and κ_d encode these modifications, depending on the mixing parameters (ϵ, ϵ_Z), the mass of the dark boson (M_{Z_D}), and the momentum transfer (Q^2). For example, ρ_d and κ_d involve terms proportional to mixing coefficients and the ratio of M_{Z_D} to the SM Z-boson mass.

The function $f\left(Q^2 / M_{Z_D}^2\right)$, which characterizes the momentum dependence, varies for different systems. For protons, f decreases with increasing Q^2, while for cesium, it is approximately constant. For instance, $f \approx 0.5$ at $M_{Z_D} \approx 2.4$ MeV and $f \approx 1$ for $M_{Z_D} \approx 100$ MeV. Using these dependencies, the model's consistency with experimental data from APV measurements provides constraints on the mixing parameters and the mass of Z_D.

In Figure 7, we plot the 3σ CL upper bound from APV on ε_Z for different values of ε. By and large, for larger values of ε, ε_Z is more constrained. Among the constraints discussed so far, APV places the strongest constraint on ε_Z in the few MeV-GeV mass range. The coupling g_D^μ which appears in Case B is unconstrained by APV. Again, because of our fine-tuned choice of g_D^e to cancel the Z_D coupling to electrons, Case C is also unconstrained by APV.

4.8. Neutrino Trident and CEνNS

Muon neutrinos can scatter off a nucleus and produce a pair of muons via a weak

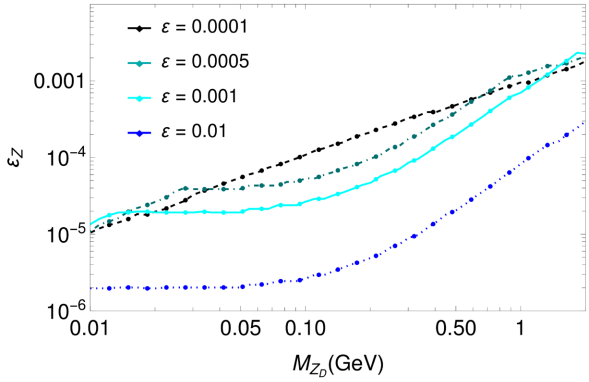

Figure 7. The 3σ CL upper bound on ε_Z from measurements of the proton and cesium weak charges in atomic parity violation experiments.

interaction known as neutrino trident production, which occurs through Z_D exchange. This process has been measured in neutrino beam experiments, such as CHARM-II [51] and CCFR [52], with results indicating a ratio of the experimental to Standard Model cross sections close to 1 for both experiments. The absence of any excess in these measurements places strong upper limits on the coupling of Z_D with muons. In particular, bounds derived for a Z' based on the $U(1)_{L_\mu - L_\tau}$ symmetry [53] are adapted to constrain the model's parameters in the M_{Z_D} and ϵ_Z plane, with the bounds being less stringent for Case A, where both vector and axial-vector interactions are involved.

Additionally, the COHERENT experiment, which observed coherent elastic neutrino-nucleus scattering (CEνNS) [54], provides further constraints on the model. The data from COHERENT set limits on the ϵ_Z parameter for a given mass of Z_D. These bounds, derived by rescaling earlier results from $U(1)_X$ models [55]-[57], turn out to be much weaker compared to direct gauge coupling constraints. For instance, for $M_{Z_D} \sim 10$ MeV, the upper bound on ϵ_Z is found to be approximately 0.0005.

4.9. Collider and Other Bounds

The dark boson Z_D can be produced through both on-shell and off-shell decays of the Z boson, such as in the process $Z \to \ell\ell Z_D$, which could lead to final states like $Z \to 4\ell$. Searches for such events at ATLAS [58] [59] and CMS [60] [61] have shown results consistent with the Standard Model, placing a lower bound on M_{Z_D} of about 5 GeV. However, due to suppression of the Z_D-lepton coupling in the model, the decay rate for $Z_D \to 4\ell$ is small, and the resulting bounds are not impactful for this model.

Belle II has also conducted a search for invisibly decaying Z' bosons in the $e^+e^- \to \mu^+\mu^-$ plus missing energy channel [62], placing an upper limit on the coupling of Z' to muons for $M_{Z'} < 6$ GeV. However, this bound is weaker than those from low-energy experiments and does not significantly constrain the model.

The dark boson could contribute to the leptonic decay width of the W boson,

particularly in processes where the Z_D decays invisibly. The contribution to the decay width is found to be small enough to be consistent with the measured W decay width. For Case A, assuming M_{Z_D} is below the dimuon threshold, the contribution is constrained to be within the uncertainty of the measured W width, setting an upper limit on ϵ_Z for different values of M_{Z_D}. This limit, however, is not as stringent as the other constraints discussed.

Additionally, LHCb searches for dark photons in dimuon samples have set strong bounds on the mixing parameter ϵ. For $M_{Z_D} \sim 200$ MeV, the bound on ϵ is ~10^{-4}, and for $M_{Z_D} \sim 2$ GeV, it is ~0.0005, which directly applies to Case A. For Cases B and C, this bound is recast in terms of the g_D^μ coupling, which rules out $g_D^\mu > 10^{-3}$ for $M_{Z_D} > 210$ MeV.

5. Parameter Fits

The study fits recent experimental data on exclusive decays ($B \to K^{(*)}\ell^+\ell^-$, $B_s^0 \to \phi\mu^+\mu^-$) and inclusive decays ($B \to X_s\ell^+\ell^-$) in different q^2 bins. The fits use the software flavio to compute both Standard Model (SM) and New Physics (NP) predictions, with the best fit values determined by minimizing the chi-squared function over the experimental data. The results are displayed in terms of 1σ, 2σ, and 3σ confidence level (CL) regions for the model parameters. The analysis excludes data below $c\bar{c}$ resonances.

In Case A, the model is constrained by bounds on the mixing parameters, ϵ and ϵ_Z, with the best fit occurring at $M_{Z_D} = 10.07$ MeV, $\epsilon = 1.6 \times 10^{-5}$, and $\epsilon_Z = 0.002$. The allowed regions for the parameters are shown in two-dimensional plots for $\left(M_{Z_D}, \epsilon_Z\right)$ and $\left(M_{Z_D}, \epsilon\right)$, with the best fit marked by a blue circle. However, the model faces tensions with low-energy constraints, particularly from atomic parity violation (APV) experiments, which exclude parameter space for $M_{Z_D} \lesssim 30$ MeV at more than 3σ. Further consideration of the dark boson's invisible decay width shows negligible impact on the fit, and the best fit remains unchanged. See Figure 8, Table 1.

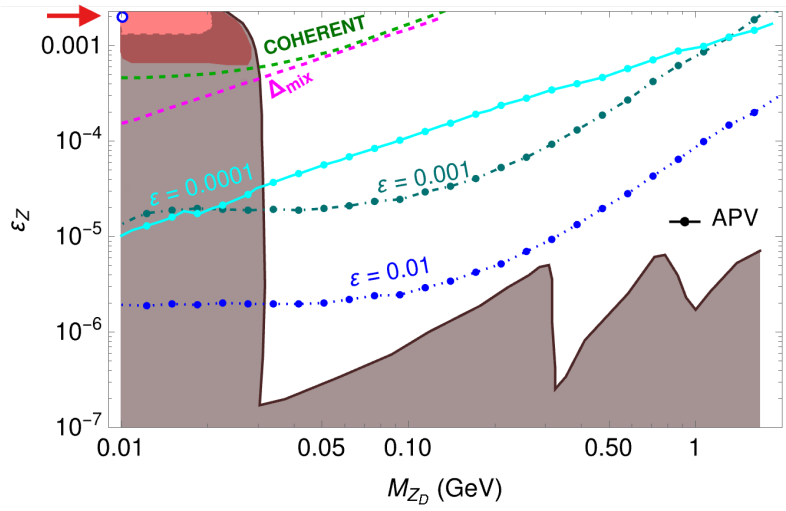

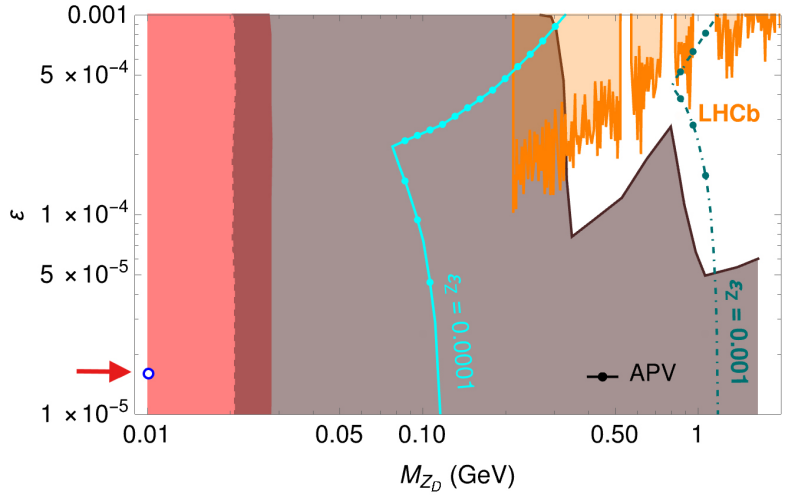

Figure 8. The 1σ (pink), 2σ (brown) and 3σ (dark brown) regions allowed by the data in Table 1 for Case A. The best fit point is marked by the blue circle. Top panel: 2σ upper limit from B_s^0 - $\bar{B}_s^0$ mixing and 1σ upper limit from COHERENT neutrino scattering data are shown by the dashed magenta and green curves, respectively. The 3σ upper limits on ε_Z from the APV measurements for $\varepsilon = 0.0001, 0.001$ and 0.01 are shown by the cyan, dark cyan and blue dotted curves, respectively. Bottom panel: The orange shaded region is excluded by LHCb dark photon searches at the 90% CL. The 3σ upper limits on ε from APV measurements for $\varepsilon_Z = 0.0001$ and 0.001 are shown by the cyan and dark cyan curves, respectively; regions to the left of the curves are excluded.

Table 1. Experimental measurements and SM expectations in q^2 bins. The SM χ^2 for the fit to all the observables is 93.56, and for just the muon modes it is 84.30.

Decay	Ref.	q^2 bin (GeV²)	Measurement	SM expectation
$\frac{d\mathcal{B}}{dq^2}(B^0 \to K^{*0}\mu^+\mu^-)\times 10^8$	[63]	0.1 - 0.98	$11.06^{+0.67}_{-0.73} \pm 0.29 \pm 0.69$	10.60 ± 1.54
		1.1 - 2.5	$3.26^{+0.32}_{-0.31} \pm 0.10 \pm 0.22$	4.66 ± 0.74
		2.5 - 4.0	$3.34^{+0.31}_{-0.33} \pm 0.09 \pm 0.23$	4.49 ± 0.70
		4.0 - 6.0	$3.54^{+0.27}_{-0.26} \pm 0.09 \pm 0.24$	5.02 ± 0.75
$\frac{d\mathcal{B}}{dq^2}(B^+ \to K^{*+}\mu^+\mu^-)\times 10^8$	[64]	0.1 - 2.0	$5.92^{+1.44}_{-1.30} \pm 0.40$	7.97 ± 1.15
		2.0 - 4.0	$5.59^{+1.59}_{-1.44} \pm 0.38$	4.87 ± 0.76
		4.0 - 6.0	$2.49^{+1.10}_{-0.96} \pm 0.17$	5.43 ± 0.74
$\frac{d\mathcal{B}}{dq^2}(B^+ \to K^+\mu^+\mu^-)\times 10^8$	[64]	0.1 - 0.98	$3.32 \pm 0.18 \pm 0.17$	3.53 ± 0.64
		1.1 - 2.0	$2.33 \pm 0.15 \pm 0.12$	3.53 ± 0.58
		2.0 - 3.0	$2.82 \pm 0.16 \pm 0.14$	3.51 ± 0.52
		3.0 - 4.0	$2.54 \pm 0.15 \pm 0.13$	3.50 ± 0.63
		4.0 - 5.0	$2.21 \pm 0.14 \pm 0.11$	3.47 ± 0.60
		5.0 - 6.0	$2.31 \pm 0.14 \pm 0.12$	3.45 ± 0.53
$\frac{d\mathcal{B}}{dq^2}(B^0 \to K^0\mu^+\mu^-)\times 10^8$	[64]	0.1 - 2.0	$1.22^{+0.59}_{-0.52} \pm 0.06$	3.28 ± 0.52

Continued

$\frac{d\mathcal{B}}{dq^2}\left(B_s^0 \to \phi\mu^+\mu^-\right)\times 10^8$	[65]	2.0 - 4.0	$1.87^{+0.55}_{-0.49} \pm 0.09$	3.25 ± 0.56
		4.0 - 6.0	$1.73^{+0.53}_{-0.48} \pm 0.09$	3.21 ± 0.54
		0.1 - 0.98	$7.74 \pm 0.53 \pm 0.12 \pm 0.37$	11.31 ± 1.34
		1.1 - 2.5	$3.15 \pm 0.29 \pm 0.07 \pm 0.15$	5.44 ± 0.61
		2.5 - 4.0	$2.34 \pm 0.26 \pm 0.05 \pm 0.11$	5.14 ± 0.73
		4.0 - 6.0	$3.11 \pm 0.24 \pm 0.06 \pm 0.15$	5.50 ± 0.69
$\mathcal{B}\left(B^+ \to K^+e^+e^-\right)\times 10^8$	[66]	0.1 - 4.0	$18.0^{+3.3}_{-3.0} \pm 0.5$	13.73 ± 1.88
		4.0 - 8.12	$9.6^{+2.4}_{-2.2} \pm 0.3$	14.11 ± 1.88
$\mathcal{B}\left(B^0 \to K^{*0}e^+e^-\right)\times 10^7$	[67]	0.03^2 - 1.0^2	$3.1^{+0.9+0.2}_{-0.8-0.3} \pm 0.2$	2.56 ± 0.44
$\mathcal{B}\left(B \to X_s\mu^+\mu^-\right)\times 10^6$	[68]	1.0 - 6.0	$0.66^{+0.82+0.30}_{-0.76-0.24} \pm 0.07$	1.67 ± 0.15
$\mathcal{B}\left(B \to X_se^+e^-\right)\times 10^6$	[68]	1.0 - 6.0	$1.93^{+0.47+0.21}_{-0.45-0.16} \pm 0.18$	1.74 ± 0.16
$\frac{d\mathcal{B}}{dq^2}\left(B^+ \to K^+e^+e^-\right)\times 10^9$	[69]	1.1 - 6.0	$25.5^{+1.3}_{-1.2} \pm 1.1$	34.9 ± 6.2
$\frac{d\mathcal{B}}{dq^2}\left(B^0 \to K^{*0}e^+e^-\right)\times 10^9$	[69]	1.1 - 6.0	$33.3^{+2.7}_{-2.6} \pm 2.2$	47.7 ± 7.5

In Case B, the direct interaction of the dark Z with muons improves the fit significantly, with the best fit occurring at $M_{Z_D} = 10.3$ MeV and $g_D^\mu = 0.28$. Despite these improvements, the model is still excluded by measurements such as $K^+ \to \mu^+\nu X$ and the W-boson width. The allowed parameter space is ruled out by these experimental constraints, as shown in the figure for Case B. A further extension with an axial-vector coupling of the dark Z to muons (Case C) leads to additional contributions, but the constraints from kaon decays and leptonic W decays impose even stricter limits, making this possibility less favorable. See Figure 9.

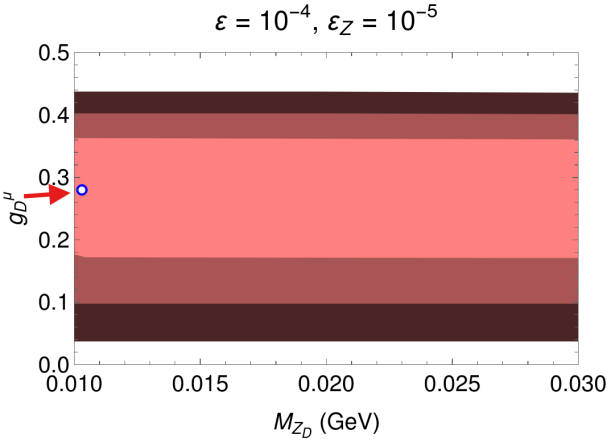

Figure 9. The 1σ, 2σ and 3σ allowed regions for Case B with the best fit point marked by a blue circle. However, the entire parameter space is ruled out by measurements of $K^+ \to \mu^+\nu X$, X = invisible / e^+e^-) and separately by the W boson width.

Case C considers a direct coupling of the dark boson to electrons, allowing the model to bypass APV constraints by fine-tuning the coupling to cancel the Z_D-electron interaction via mixing. The best fit point occurs at $M_{Z_D} = 30.2$ MeV and $g_D^\mu = 0.033$. This scenario provides a marked improvement over Case B, with a better fit to the binned $b \to s\mu^+\mu^-$ data and an order of magnitude smaller g_D^μ. The parameter space remains consistent with bounds from neutrino trident production, $K \to \mu +$ invisible, and the W-boson width. The allowed region, which fits the data at 2σ CL, is also shown in the figure for Case C, where dark photon searches at LHCb further constrain the parameter space. See Figure 10.

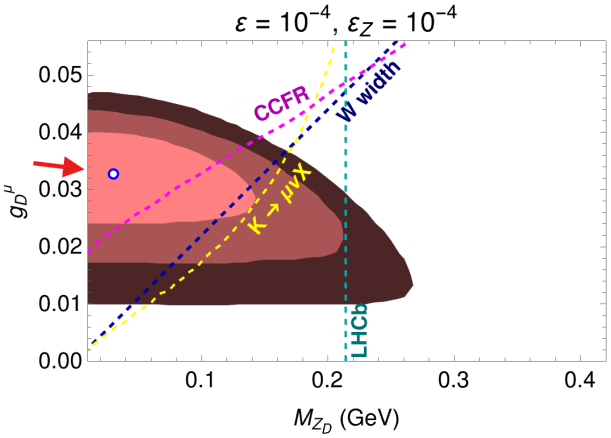

Figure 10. The 1σ, 2σ and 3σ allowed regions for Case C with the best fit point marked by a blue circle. Upper limits from neutrino trident production at CCFR (at 95% CL), $K \to \mu\nu X$ (at 90% CL) and the W width (at 95% CL) are shown by the dashed magenta, yellow and dark blue curves, respectively. Dark photon searches at LHCb rule out the region to the right of the vertical dashed dark cyan line at 90% CL.

6. Summary

This study investigates the contributions of a dark photon and dark Z boson to $b \to s\ell^+\ell^-$ decays, focusing on their effects on the decay amplitudes and incorporating hadronic decays of the dark boson. By fitting to experimental data, we estimate the mass and mixing parameters of the dark boson.

Two extensions of the model, where the dark Z couples directly to muons or electrons, improve the fit to the data. However, the viable parameter space is significantly constrained by other experimental results, especially the anomalous magnetic moment of the muon.

In Case A, the model requires a dark boson mass of less than 30 MeV and specific mixing parameters, but the parameter space is excluded by atomic parity violation experiments. For larger masses, stringent constraints from flavor-changing neutral currents limit the model further.

Case B adds a direct muon coupling, but this results in the exclusion of the entire parameter space due to enhancements in processes like $K \to \mu\nu X$ and the W boson width.

Case C refines the model by introducing a fine-tuned electron coupling, which cancels the electron-mixing contribution, allowing the model to bypass previous constraints. A small viable region remains, but reconciling this with the muon anomalous magnetic moment requires additional new physics.

Conflicts of Interest

The author declares no conflicts of interest regarding the publication of this paper.

References

[1] Holdom, B. (1986) Two U(1)'s and E Charge Shifts. *Physics Letters B*, **166**, 196-198. https://doi.org/10.1016/0370-2693(86)91377-8

[2] Gopalakrishna, S., Jung, S. and Wells, J.D. (2008) Higgs Boson Decays to Four Fermions through an Abelian Hidden Sector. *Physical Review D*, **78**, Article ID: 055002. https://doi.org/10.1103/physrevd.78.055002

[3] Davoudiasl, H., Lee, H. and Marciano, W.J. (2012) "Dark" Zimplications for Parity Violation, Rare Meson Decays, and Higgs Physics. *Physical Review D*, **85**, Article ID: 115019. https://doi.org/10.1103/physrevd.85.115019

[4] Datta, A., Liao, J. and Marfatia, D. (2017) A Light Z' for the R_K Puzzle and Nonstandard Neutrino Interactions. *Physics Letters B*, **768**, 265-269. https://doi.org/10.1016/j.physletb.2017.02.058

[5] Sala, F. and Straub, D.M. (2017) A New Light Particle in B Decays? *Physics Letters B*, **774**, 205-209. https://doi.org/10.1016/j.physletb.2017.09.072

[6] Bishara, F., Haisch, U. and Monni, P.F. (2017) Regarding Light Resonance Interpretations of the B Decay Anomalies. *Physical Review D*, **96**, Article ID: 055002. https://doi.org/10.1103/physrevd.96.055002

[7] Ghosh, D. (2017) Explaining the R_K and R_{K^*} Anomalies. *The European Physical Journal C*, **77**, Article No. 694. https://doi.org/10.1140/epjc/s10052-017-5282-y

[8] Datta, A., Kumar, J., Liao, J. and Marfatia, D. (2018) New Light Mediators for the R_K and R_{K^*} Puzzles. *Physical Review D*, **97**, Article ID: 115038.

[9] Altmannshofer, W., Baker, M.J., Gori, S., Harnik, R., Pospelov, M., Stamou, E., *et al.* (2018) Light Resonances and the Low-q^2 Bin of R_{K^*}. *Journal of High Energy Physics*, **2018**, Article No. 188. https://doi.org/10.1007/jhep03(2018)188

[10] Datta, A., Dutta, B., Liao, S., Marfatia, D. and Strigari, L.E. (2019) Neutrino Scattering and B Anomalies from Hidden Sector Portals. *Journal of High Energy Physics*, **2019**, Article No. 91. https://doi.org/10.1007/jhep01(2019)091

[11] Datta, A., Kumar, J. and London, D. (2019) The B Anomalies and New Physics in $b \to se^+e^-$. *Physics Letters B*, **797**, Article ID: 134858. https://doi.org/10.1016/j.physletb.2019.134858

[12] Darmé, L., Fedele, M., Kowalska, K. and Sessolo, E.M. (2020) Flavour Anomalies from a Split Dark Sector. *Journal of High Energy Physics*, **2020**, Article No. 148. https://doi.org/10.1007/jhep08(2020)148

[13] Borah, D., Mukherjee, L. and Nandi, S. (2020) Low Scale $U(1)_X$ Gauge Symmetry as an Origin of Dark Matter, Neutrino Mass and Flavour Anomalies. *Journal of High Energy Physics*, **2020**, Article No. 52. https://doi.org/10.1007/jhep12(2020)052

[14] Darmé, L., Fedele, M., Kowalska, K. and Sessolo, E.M. (2022) Flavour Anomalies and

the Muon g-2 from Feebly Interacting Particles. *Journal of High Energy Physics*, **2022**, Article No. 85. https://doi.org/10.1007/jhep03(2022)085

[15] Crivellin, A., Manzari, C.A., Altmannshofer, W., Inguglia, G., Feichtinger, P. and Martin Camalich, J. (2022) Towards Excluding a Light Z' Explanation of $b \to s\ell^+\ell^-$. *Physical Review D*, **106**, L031703.

[16] Xu, F. (2015) Dark Z Implication for Flavor Physics. *Journal of High Energy Physics*, **2015**, Article No. 170. https://doi.org/10.1007/jhep06(2015)170

[17] Bertuzzo, E., Jana, S., Machado, P.A.N. and Zukanovich Funchal, R. (2019) Neutrino Masses and Mixings Dynamically Generated by a Light Dark Sector. *Physics Letters B*, **791**, 210-214. https://doi.org/10.1016/j.physletb.2019.02.023

[18] Bertuzzo, E., Jana, S., Machado, P.A.N. and Zukanovich Funchal, R. (2018) Dark Neutrino Portal to Explain Miniboone Excess. *Physical Review Letters*, **121**, Article ID: 241801. https://doi.org/10.1103/physrevlett.121.241801

[19] Link, J.M. and Xu, X. (2019) Searching for BSM Neutrino Interactions in Dark Matter Detectors. *Journal of High Energy Physics*, **2019**, Article No. 4. https://doi.org/10.1007/jhep08(2019)004

[20] Bednyakov, A.V. and Tanyıldızı, Ş.H. (2015) A Mathematica Package for Calculation of One-Loop Penguins in FCNC Processes. *International Journal of Modern Physics C*, **26**, Article ID: 1550042. https://doi.org/10.1142/s0129183115500424

[21] Tulin, S. (2014) New Weakly Coupled Forces Hidden in Low-Energy QCD. *Physical Review D*, **89**, Article ID: 114008. https://doi.org/10.1103/physrevd.89.114008

[22] Ilten, P., Soreq, Y., Williams, M. and Xue, W. (2018) Serendipity in Dark Photon Searches. *Journal of High Energy Physics*, **2018**, Article No. 4. https://doi.org/10.1007/jhep06(2018)004

[23] Foguel, A.L., Reimitz, P. and Funchal, R.Z. (2022) A Robust Description of Hadronic Decays in Light Vector Mediator Models. *Journal of High Energy Physics*, **2022**, Article No. 119. https://doi.org/10.1007/jhep04(2022)119

[24] Particle Data Group Collaboration (2022) Review of Particle Physics. *Progress of Theoretical and Experimental Physics*, **2022**,Article ID: 083C01.

[25] Amaral, D.W.P., Cerdeño, D.G., Cheek, A. and Foldenauer, P. (2021) Confirming $U(1)_{L_\mu - L_\tau}$ as a Solution for $(g-2)_\mu$ with Neutrinos. *The European Physical Journal C*, **81**, Article No. 861. https://doi.org/10.1140/epjc/s10052-021-09670-z

[26] Nomura, T., Okada, H. and Yun, S. (2021) Vector dark matter from a gauged SU(2) symmetry. *Journal of High Energy Physics*, **2021**, Article No. 122. https://doi.org/10.1007/jhep06(2021)122

[27] Artuso, M., Borissov, G. and Lenz, A. (2016) CP Violation in the B_s^0 System. *Reviews of Modern Physics*, **88**, Article ID: 045002. https://doi.org/10.1103/revmodphys.88.045002

[28] Lattice, F. and MILC collaboration (2016) $B_{(s)}^0$-Mixing Matrix Elements from Lattice QCD for the Standard Model and Beyond. *Physical Review D*, **93**, Article ID: 113016.

[29] Buchalla, G., Buras, A.J. and Lautenbacher, M.E. (1996) Weak Decays Beyond Leading Logarithms. *Reviews of Modern Physics*, **68**, 1125-1244. https://doi.org/10.1103/revmodphys.68.1125

[30] Aoki, Y., *et al.* (2021) FLAG Review 2021. arXiv: 2111.09849.

[31] Di Luzio, L., Kirk, M., Lenz, A. and Rauh, T. (2019) ΔM_s Theory Precision Confronts Flavour Anomalies. *Journal of High Energy Physics*, **2019**, Article No. 9.

https://doi.org/10.1007/jhep12(2019)009

[32] Aoki, S., Aoki, Y., Bečirević, D., Blum, T., Colangelo, G., Collins, S., *et al.* (2020) FLAG Review 2019. *The European Physical Journal C*, **80**, Article No. 113. https://doi.org/10.1140/epjc/s10052-019-7354-7

[33] Altmannshofer, W. and Stangl, P. (2021) New Physics in Rare B Decays after Moriond 2021. *The European Physical Journal C*, **81**, Article No. 952. https://doi.org/10.1140/epjc/s10052-021-09725-1

[34] Guadagnoli, D., Langenbruch, C. and Manoni, E. (2023). WG3 Summary—Rare B, D and K Decays. *Proceedings of* 11*th International Workshop on the CKM Unitarity Triangle—PoS*(*CKM*2021), 22-26 November 2021, 1-25. https://doi.org/10.22323/1.411.0014

[35] Aaij, R., *et al.* (2022) Measurement of the $B_s^0 \to \mu^+\mu^-$ Decay Properties and Search for the $B^0 \to \mu^+\mu^-$ and $B_s^0 \to \mu^+\mu^-\gamma$ Decays. *Physical Review D*, **105**, Article ID: 012010.

[36] Fuyuto, K., Hou, W. and Kohda, M. (2016) z'-Induced FCNC Decays of Top, Beauty, and Strange Quarks. *Physical Review D*, **93**, Article ID: 054021. https://doi.org/10.1103/physrevd.93.054021

[37] Ball, P. and Zwicky, R. (2005) New Results on $B_{d,s} \to \rho, \omega, K^*, \phi$ Decay Form Factors from Light-Cone Sum Rules. *Physical Review D*, **71**, Article ID: 014015. https://doi.org/10.1103/physrevd.71.014015

[38] Felkl, T., Li, S.L. and Schmidt, M.A. (2021) A Tale of Invisibility: Constraints on New Physics in $b \to s\nu\nu$. *Journal of High Energy Physics*, **2021**, Article No. 118. https://doi.org/10.1007/jhep12(2021)118

[39] Dattola, F. (2021) Search for $B^+ \to K^+\nu\bar{\nu}$ Decays with an Inclusive Tagging Method at the Belle II Experiment. arXiv: 2105.05754.

[40] Grygier, J., *et al.* (2017) Search for $\boldsymbol{B \to h\nu\bar{\nu}}$ Decays with Semileptonic Tagging at Belle. *Physical Review D*, **96**, Article ID: 091101.

[41] Kucerova, Z. (2022) Measurement of the Very Rare $K^+ \to \pi^+\nu\bar{\nu}$ Decay. *Nuclear and Particle Physics Proceedings*, **318-323**, 160-164.

[42] Ahn, J.K., *et al.* (2021) Study of the $K_L \to \pi^0\nu\bar{\nu}$ Decay at the J-PARC KOTO Experiment. *Physical Review Letters*, **126**, Article ID: 121801.

[43] Buras, A.J., Buttazzo, D., Girrbach-Noe, J. and Knegjens, R. (2015) $K^+ \to \pi^+\nu\bar{\nu}$ and $K_L \to \pi^0\nu\bar{\nu}$ in the Standard Model: Status and Perspectives. *Journal of High Energy Physics*, **2015**, Article No. 33. https://doi.org/10.1007/jhep11(2015)033

[44] Particle Data Group Collaboration (2024) Review of Particle Physics.

[45] Grossman, Y. and Nir, Y. (1997) $K_L \to \pi^0\nu\nu$ beyond the Standard Model. *Physics Letters B*, **398**, 163-168. https://doi.org/10.1016/s0370-2693(97)00210-4

[46] NA62 Collaboration (2021) Search K^+ for Decays to a Muon and Invisible Particles. *Physics Letters B*, **816**, Article ID: 136259.

[47] Poblaguev, A.A., *et al.* (2002) Experimental Study of the Radiative Decays K+ -> mu+ nu e+ e- and K+ -> e+ nu e+ e-. *Physical Review Letters*, 89, Article ID: 061803.

[48] Aguilar-Arevalo, A., *et al.* (20211) Search for Three Body Pion Decays $\pi^+ \to l^+\nu X$. *Physical Review D*, **103**, Article ID: 052006.

[49] The Jefferson Lab Qweak Collaboration (2018) Precision Measurement of the Weak Charge of the Proton. *Nature*, **557**, 207-211. https://doi.org/10.1038/s41586-018-0096-0

[50] Wood, C.S., Bennett, S.C., Cho, D., Masterson, B.P., Roberts, J.L., Tanner, C.E., *et al.* (1997) Measurement of Parity Nonconservation and an Anapole Moment in Cesium. *Science*, **275**, 1759-1763. https://doi.org/10.1126/science.275.5307.1759

[51] Geiregat, D., *et al.* (1990) First Observation of Neutrino Trident Production. *Physics Letters B*, **245**, 271-275.

[52] Mishra, S.R., *et al.* (1991) Neutrino Tridents and W Z Interference. *Physical Review Letters*, **66**, Article No. 3117.

[53] Altmannshofer, W., Gori, S., Martín-Albo, J., Sousa, A. and Wallbank, M. (2019) Neutrino Tridents at Dune. *Physical Review D*, **100**, Article ID: 115029. https://doi.org/10.1103/physrevd.100.115029

[54] Akimov, D., *et al.* (2017) Observation of Coherent Elastic Neutrino-Nucleus Scattering. *Science*, **357**, 1123-1126.

[55] Han, T., Liao, J., Liu, H. and Marfatia, D. (2019) Nonstandard Neutrino Interactions at COHERENT, DUNE, T2HK and LHC. *Journal of High Energy Physics*, **2019**, Article No. 28. https://doi.org/10.1007/jhep11(2019)028

[56] Banerjee, H., Dutta, B. and Roy, S. (2021) Probing Lμ-Lτ Models with CEνNS: A New Look at the Combined COHERENT CsI and Ar Data. *Physical Review D*, **104**, Article ID: 015015.

[57] Corona, M.A., Cadeddu, M., Cargioli, N., Dordei, F., Giunti, C., Li, Y.F., *et al.* (2022) Probing Light Mediators and $(g-2)_\mu$ through Detection of Coherent Elastic Neutrino Nucleus Scattering at Coherent. *Journal of High Energy Physics*, **2022**, Article No. 109. https://doi.org/10.1007/jhep05(2022)109

[58] Aad, G., *et al.* (2014) Measurements of Four-Lepton Production at the Z Resonance in *pp* Collisions at $\sqrt{s}=7$ and 8 TeV with ATLAS. *Physical Review Letters*, **112**, Article ID: 231806.

[59] ATLAS Collaboration (2023) Search for a New Z' Gauge Boson in 4μ Events with the ATLAS Experiment. arXiv: 2301.09342.

[60] CMS Collaboration (2012) Observation of Z Decays to Four Leptons with the CMS Detector at the LHC. arXiv: 1210.3844.

[61] CMS Collaboration (2019) Search for an $L_\mu - L_\tau$ Gauge Boson Using $Z \to 4\mu$ Events in Proton-Proton Collisions at $\sqrt{s}=13$ TeV. *Physics Letters B*, **792**, 345-368.

[62] Adachi, I., *et al.* (2020) Search for an Invisibly Decaying Z' Boson at Belle II $e^+e^- \to \mu^+\mu^-\left(e^\pm\mu^\mp\right)$ in Plus Missing Energy Final States. *Physical Review Letters*, **124**, Article ID: 141801.

[63] Aaij, R., *et al.* (2016) Measurements of the S-Wave Fraction in $B^0 \to K^+\pi^-\mu^+\mu^-$ Decays and the $B^0 \to K^*(892)^0\mu^+\mu^-$ Differential Branching Fraction. *Journal of High Energy Physics*, **11**, 47.

[64] Aaij, R., *et al.* (2014) Differential Branching Fractions and Isospin Asymmetries of $B \to K^{(*)}\mu^+\mu^-$ Decays. *Journal of High Energy Physics*, **2014**, Article No. 133.

[65] Aaij, R., *et al.* (2021) Branching Fraction Measurements of the Rare $B_s^0 \to \phi\mu^+\mu^-$ and $B_s^0 \to f_2'(1525)\mu^+\mu^-$-Decays. *Physical Review Letters*, **127**, Article ID: 151801.

[66] Choudhury, S., *et al.* (2021) Test of Lepton Flavor Universality and Search for Lepton Flavor Violation in $B \to K\ell\ell$ Decays. *Journal of High Energy Physics*, **2021**, Article No. 105.

[67] Aaij, R., *et al.* (2013) Measurement of the $B^0 \to K^{*0} e^+ e^-$ Branching Fraction at Low Dilepton Mass. *Journal of High Energy Physics*, **2013**, Article No. 159.

[68] Lees, J.P., *et al.* (2014) Measurement of the $B \to X_s l^+ l^-$ Branching Fraction and Search for Direct CP Violation from a Sum of Exclusive Final States. *Physical Review Letters*, **112**, Article ID: 211802.

[69] Aaij, R., *et al.* (2023) Measurement of Lepton Universality Parameters in $B^+ \to K^+ \ell^+ \ell^-$ and $B^0 \to K^{*0} \ell^+ \ell^-$ Decays. *Physical Review D*, **108**, Article ID: 032002.